

Article

Role of Lifshitz Invariants in Liquid Crystals

Amelia Sparavigna

Dipartimento di Fisica, Politecnico di Torino, C.so Duca degli Abruzzi 24, Torino, Italy;
E-Mail: amelia.sparavigna@polito.it; Tel. +39-011-564-7360; Fax: +39-011-564-7399

Received: 5 May 2009; in revised form: 12 June 2009 / Accepted: 16 June 2009 /

Published: 16 June 2009

Abstract: The interaction between an external action and the order parameter, via a dependence described by a so-called Lifshitz invariant, is very important to determine the final configuration of liquid crystal cells. The external action can be an electric field applied to the bulk or the confinement due to free surfaces or cell walls. The Lifshitz invariant includes the order parameter in the form of an elastic strain. This coupling between elastic strains and fields, inserted in a Landau-Ginzburg formalism, is well known and gives rise to striction effects causing undulations in the director configuration. We want to discuss here the role of Lifshitz coupling terms, following an approach similar to that introduced by Dzyaloshinskii for magnetic materials. Case studies on nematics in planar and cylindrical cells are also proposed.

Keywords: liquid crystals; nematics; confined nematics

1. Introduction

The contributions to the free-energy density of terms in the derivatives of order parameter are of great importance and recognised to be fundamental in governing the appearance of spatially modulated structures in magnetic materials and of periodic patterns in liquid crystals. It is possible to identify the same structure in the free energy, when it is represented by a Landau-Lifshitz phenomenological theory of phase transitions; this structure has the form of an invariant term, so-called Lifshitz invariant, which is linear with respect to the gradient of order parameter. As shown by Landau and Lifshitz [1], a system near its phase transition point may be unstable with respect to distortions of the appropriate

order parameter. This instability may develop, when the irreducible representation allows a quadratic antisymmetric combination, linear in the order parameter components and in their gradients.

Phases with large-scale space fluctuations of the order parameter were discovered experimentally in the 1960's [2]. Using the approach proposed by Lifshitz, Dzyaloshinskii [3] showed that these configurations are associated with the development of instabilities and found the corresponding approximate solutions of the phase equations. Presently, the family of experimentally observed modulated states has grown both in magnetic and liquid crystal systems [4-7].

The aim of this paper is to discuss those properties and behaviours of liquid crystal materials originated by Lifshitz contributes to the free energy. Before the discussion of Lifshitz invariants in liquid crystals, we prefer to devote a section of the paper to a brief remark on the use of these invariants in magnetic systems. After this remark, we show how the flexoelectric effect, the chiral elastic term and the saddle-splay surface contribution can be described as Lifshitz contributions.

A liquid-crystal material, the free-energy of which contains a Lifshitz term coupling elastic strains and external fields, can exhibit undulations in the director configuration. Periodic structures in liquid crystal materials can be achieved either in cholesteric or ferroelectric liquid crystals, which possess a natural periodic helicoidal distribution of the molecular orientation. In a nematic liquid crystal cell, a periodic structure can appear spontaneously too, with period that can be controlled by external factors such as applied fields and asymmetric anchoring conditions. The electric field controls the instability produced by the flexoelectric effect. Flexoelectric domains were first observed by Vistin and theoretically studied by Bobylev and Pikin [8,9]. More recently, Lavrentovich and Pergamenschick discovered another interesting instability in nematics, controlled by the saddle-splay surface contribution to the free energy [10,11].

In the final part of this paper, we propose a detailed discussion of some case studies involving flexoelectricity. In particular, we discuss the hybrid nematic cell in planar geometry and show its complete phase diagrams. The same we shall do for the cylindrical confinement of nematics. To the author's knowledge, the problem of flexoelectricity in cylindrical confinement has not been discussed before: in the framework of its approximate solution, the corresponding phase diagram shows instabilities. The discussion on saddle-splay instabilities concludes the paper.

2. The Dzyaloshinskii-Moriya Coupling

Some magnetic structures are characterised by a modulation of the spin arrangements over periods, which are long compared to the size of the lattice cell and usually not commensurate with it. The existence of such magnetic structures can be due to competition between exchange interactions or to relativistic effects like spin-orbit coupling. Relativistic interactions were first considered by Dzyaloshinskii [3] and received a microscopic description by Moriya [12]. The Dzyaloshinskii-Moriya (DM) interaction can be written as a product of three vectors, $F_{DM} = \vec{D} \cdot (\vec{S}_i \times \vec{S}_j)$, where \vec{D} is the DM-vector and \vec{S}_i, \vec{S}_j are spin vectors. The bond symmetry determines the direction of the DM-vector whereas the strength of the spin-orbit coupling gives its intensity [12,13].

The macroscopic manifestation of the antisymmetric DM couplings takes place in non-centrosymmetric magnetic crystals. Dzyaloshinskii showed that, in this case, the DM interaction

stabilises long-periodic spatially modulated structures of the vectors \vec{S}_i , structures with a fixed sense of rotation. In antiferromagnets, the DM-interaction favours arrangements of the magnetic moments, which result in a weak spontaneous magnetisation.

Within a continuum approximation for magnetic properties, the interactions responsible for these modulations are expressed by inhomogeneous invariants. In Ref. [14], these contributions to the free magnetic energy, involving first derivatives of magnetisation with respect to spatial coordinates, are defined as the inhomogeneous Dzyaloshinskii-Moriya interactions. These interactions are linear with respect to first spatial derivatives of magnetisation \vec{M} in an antisymmetric mathematical form, firstly studied in the theory of phase transitions by E. M. Lifshitz and known as Lifshitz invariants. Spiral structures arise in magnetic systems from the presence of the Lifshitz invariant in the free energy [15].

The structure of the Lifshitz invariant is, in the case of the inhomogeneous Dzyaloshinskii-Moriya interaction, a product of three vectors: a vector \vec{D} representing an internal or external field or a fixed direction in the space, a vector \vec{M} representing the local order parameter and the $\vec{\nabla}$ operator on the order parameter components. The product has the following form:

$$f_L = \vec{D} \cdot [\vec{M}(\vec{\nabla} \cdot \vec{M}) - (\vec{M} \cdot \vec{\nabla})\vec{M}] \quad (1)$$

In the case of the liquid crystals, we shall see that vector \vec{D} can be an external electric field or the direction perpendicular to the sample surface. It is better to remark that in Ref.4, we can find another choice for the DM interaction, as the pseudoscalar $f_{DM} = D[\vec{M} \cdot \vec{\nabla} \times \vec{M}]$. We will discuss this form in the Sect.5, concerning the chiral nematics.

We used the DM interactions in 1996 to study the field-induced phase transition of BiFeO₃ [16]. More recently, the coupling of spin waves with the optical phonons has been discussed in the framework of Lifshitz invariant, for the same material [17]. An antiferromagnetic vector \vec{L} characterises the BiFeO₃ spin structure. The Landau-Ginzburg energy density [3] of the spin structure is the following sum of four terms:

$$\begin{aligned} f &= f_L + f_{exch} + f_u + f_{ME} = \\ &= -\alpha P_{z,S} (L_x \nabla_x L_z + L_y \nabla_y L_z) + A \sum_{i=x,y,z} (\nabla L_i)^2 - K_u L_z^2 - \beta \vec{E} \cdot \vec{H}_{DM} \end{aligned} \quad (2)$$

The first term f_L in Equation 2 is the magneto-electric coupling as a Lifshitz invariant, where $P_{z,S}$ is the z-component of the spontaneous polarization vector, and α is the inhomogeneous relativistic exchange constant (inhomogeneous magneto-electric constant). The Lifshitz invariant is the responsible for the spatially modulated spin structure in BiFeO₃, as shown in Ref.16. The second term f_{exch} in (2) is the inhomogeneous exchange energy, where A is a stiffness constant. In the third term, K_u is the uniaxial anisotropy. f_{ME} is the coupling of an external electric field \vec{E} with a spatial uniform inner field $\vec{H}_{DM} = \vec{d} \times \vec{L}$, where $\vec{d} = (0,0,P_z)$, and β the homogeneous magneto-electric constant. This term is originated from a magneto-electric-like DM interaction.

The first term of the free energy can be rewritten, using the following vector:

$$\vec{A} = \vec{L}(\vec{\nabla} \cdot \vec{L}) - (\vec{L} \cdot \vec{\nabla})\vec{L} \quad (3)$$

in the form:

$$f_L = -\alpha \vec{P}_S \cdot \vec{A} \quad (4)$$

as a scalar product of two fields. In our paper [16], we investigated the influence of an electric field on the spatially modulated spin structure (SDW state). The electric field has a tendency to prefer a homogeneous state and to induce a phase transition to this state. In that paper, we used the analogy with nematic liquid crystals to study magnetic materials. Here, we want to enhance the analogy of liquid crystal interactions with the two form of the Dzyaloshinskii-Moriya DM interaction.

3. The Flexoelectricity in Liquid Crystals

Let us consider a nematic liquid crystal and assume as order parameter the director field \vec{n} , describing the local mean orientation of molecules. This is usually a unit vector. Vector \vec{A} can be used in nematics too, rewritten in the following form:

$$\vec{A} = \vec{n}(\vec{\nabla} \cdot \vec{n}) - (\vec{n} \cdot \vec{\nabla})\vec{n} = \vec{n} \operatorname{div} \vec{n} + \vec{n} \times \operatorname{rot} \vec{n} \quad (5)$$

Vector \vec{A} in Equation 5 is well known in the physics of liquid crystals. \vec{A} is encountered in the structure of flexoelectric contribution to bulk free energy as $f_{Flexo} = -\vec{P} \cdot \vec{E}$. Flexoelectricity is a property of liquid crystals similar to the piezoelectric effect. In certain anisotropic materials, which contain molecular asymmetry or quadrupolar ordering with permanent molecular dipoles, an applied electric field may induce an orientational distortion. Conversely any distortion will induce a macroscopic polarization within the material. The polarization vector \vec{P} in the flexoelectric term is then described with a distortion in the nematic director field:

$$\vec{P} = e_S \vec{n}(\vec{\nabla} \cdot \vec{n}) - e_B (\vec{n} \cdot \vec{\nabla})\vec{n} = e_S \vec{n} \operatorname{div} \vec{n} + e_B \vec{n} \times \operatorname{rot} \vec{n} \quad (6)$$

The two terms in the polarization vector are due to the splay and the bend contribution. The coupling of the polarization \vec{P} with an external electric field results in the appearance of a periodic distortion of an initial planar orientation of the nematic cell [18]. Meyer showed that the infinite liquid crystal must be disturbed, the perturbation is periodic along the director orientation and the period is inversely proportional to electric field strength [19]. This is not surprising because the polarization vector \vec{P} has the same structure of vector \vec{A} in Equation 5.

In flexoelectricity, the polarization is induced by a deformation of the director field. Let us remember that in the piezoelectric materials, an applied uniform strain can induce an electric polarization or vice versa. Crystallographic considerations restrict this property to non-centrosymmetric systems. A strain, which is not uniform, can potentially break the inversion symmetry and induce polarization in non-piezoelectric materials. While the conventional piezoelectric property is different from zero only for certain select materials, the non-local coupling of strain and polarization could be potentially found in all dielectrics [20]. As a result, we find that the coupling with an external field gives the Lifshitz invariant as a DM non homogenous coupling for the electric field with the Lifshitz vector.

4. Periodic Distortions in Nematics

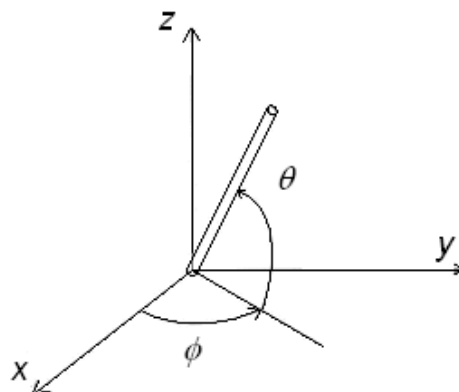
Let us discuss more deeply the Meyer result [18,19] of a periodic distortion in the infinite medium. The free energy density is given by:

$$f = \frac{1}{2}K \left[(\text{div } \vec{n})^2 + (\vec{n} \cdot \text{rot } \vec{n})^2 + (\vec{n} \times \text{rot } \vec{n})^2 \right] - e \vec{E} \cdot (\vec{n} \text{ div } \vec{n} + \vec{n} \times \text{rot } \vec{n}) \quad (7)$$

in the uniform elastic approximation, with K elastic constant, and with the dielectric anisotropy negligible. Moreover we assume $e_B \approx e_S \approx e$. Let us consider the director \vec{n} in a uniform configuration, as a vector parallel to x -axis and the electric field \vec{E} parallel to z -axis as $\vec{E} = E \vec{k}$, where \vec{k} is the unit vector of z -axis. Angles θ and ϕ are shown in the Figure 1.

The components of director \vec{n} are $n_x = \cos\theta$, $n_y = 0$, $n_z = \sin\theta$, if $\phi = 0$. Let us consider a deformation of \vec{n} depending on x , to see what happens. In fact, we want to give just a very rough approach to the problem. In the case of an infinite nematic medium without deformations of the director, the free energy density is zero. If we had a tilt angle variation of the form $\theta = -e x E / K$, we should have a periodic deformation of director \vec{n} .

Figure 1. The frame of reference and the angles used to describe the director, represented by the rod-like molecule.



The free energy density, including the flexoelectric term, is:

$$f_{\text{distorted}} = \frac{1}{2}K \left(\frac{\partial \theta}{\partial x} \right)^2 + e E \frac{\partial \theta}{\partial x} = -\frac{1}{2}e \frac{E^2}{K} < 0 \quad (8)$$

Then, a periodic distortion in a non-confined nematic is possible because it has a free energy density lower than that possessed by the uniform configuration. There is not a threshold for the electric field, since the existence of a threshold is a consequence of the medium confinement.

Let us imagine a nematic material confined in a cell composed by two plane walls, parallel to $[x,y]$ plane, at a distance d . The anchoring conditions must be included in the energy balance. We can assume a surface energy density of the Rapini-Papoular form $f = -W \cos^2 \theta$, for a surface treatment favouring a molecular alignment parallel with the x -axis. If the director field \vec{n} is uniform in the planar alignment, $f = -W$. Let us choose, as in Ref. [18], the behaviour of the tilt angle in the form

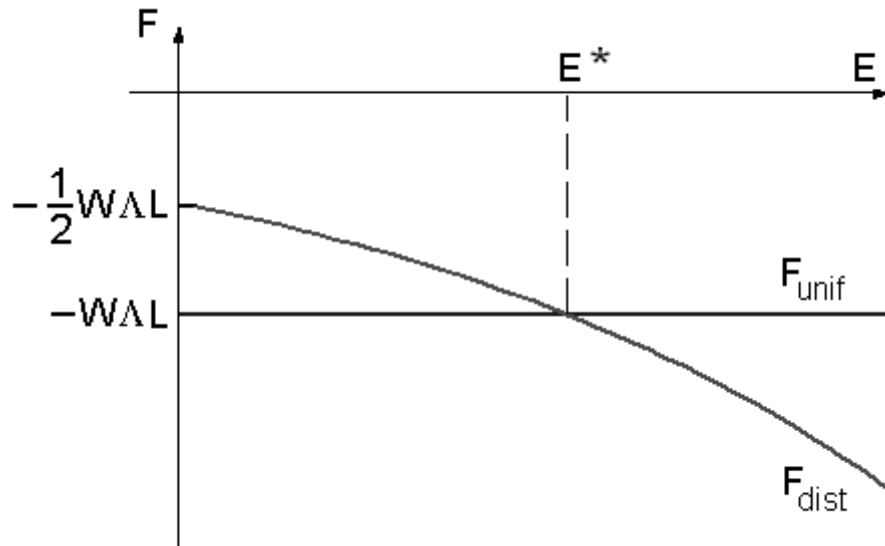
$\theta = -\alpha xE/K$, with α , a coefficient with dimensions *charge/length*. The free energy density is given as in Equation 8.

Integrating the free energy density on the cell volume $V = d \Lambda L$, where d is the cell thickness, L a fixed length in y -direction and Λ the director distortion wavelength along the x -direction, we obtain:

$$F_{distorted} = E^2 \frac{d\Lambda L}{K} \left[\frac{1}{2} \alpha^2 - e\alpha \right] - \frac{1}{2} W \Lambda L \tag{9}$$

The last term in (9) is the surface energy contribution. In the case of a uniform director field, we have a total energy as $F_{uniform} = -W \Lambda L$. The behaviour of the two free energies $F_{distorted}, F_{uniform}$ is given in Figure 2: we can see the existence of a threshold field E^* .

Figure 2. Comparison of the free energy behaviours in the case of the uniform configuration and for the distorted one.



If the electric field has a value $E < E^*$, the stable configuration of the director field is that with lower energy, in this case, when the director field is uniform. When $E > E^*$, the stable configuration is the distorted one.

Comparing the two values of the total energy, that is:

$$F_{distorted} \approx F_{uniform}, \tag{10}$$

we can approximately find the threshold electric field as:

$$(E^*)^2 \left(\frac{1}{2} \alpha^2 d - e\alpha d \right) = -\frac{W}{2} K \tag{11}$$

where $(\alpha^2 d / 2 - e\alpha d) < 0$, to have a real electric field:

$$(E^*)^2 = \frac{W}{d} \frac{K}{|\alpha^2 - 2e\alpha|} \tag{12}$$

The threshold field has a value:

$$E^* = \left(\frac{WK}{\alpha d |\alpha - 2e|} \right)^{1/2} = \left(\frac{WK}{a^2 d} \right)^{1/2} \quad (13)$$

where $\alpha < 2e$. Estimating $a^2 = |\alpha(\alpha - 2e)| \approx e^2$ and assuming the parameter values $W = 10^{-4} \text{ J/m}^2$, $K = 10^{-11} \text{ N}$, $d = 10 \text{ }\mu\text{m}$, $a = 10^{-11} \text{ C/m}$ we find a threshold voltage of $\approx 10 \text{ Volt}$.

5. The Chiral Nematic and the Smectic Phase

Much research has taken place in the field of liquid crystals to find ferroelectric materials, from the earlier studies on the smectic phases till the more recent banana-like materials [20-23]. The smectic phases are organised in layers. There are three main smectic phases: A, C and C*. In the smectic C (SmC) phase the director \vec{n} is tilted by a fixed angle, with respect to the layer normal \vec{v} . The chiral smectic (SmC*) phase shows in addition an intrinsic twist of the director from layer to layer. The symmetry breaking $C_{2h} \rightarrow C_2$ allows molecular electric dipoles to form a spontaneous electric polarization \vec{P} , which lies in the smectic planes. The macroscopic polarization vanishes in the SmC* phase, but an electric field parallel to the layers can distort the helicoidal structure, disfavouring SmC* and leading to a phase with a macroscopic polarization. In the Landau theory of smectic liquid crystals, the free energy is expanded in two order parameters: the projection \vec{n} of the director onto the smectic layer plane and the layer polarization \vec{P} [24]. The chiral term, responsible of the SmC* phase has in [20] the structure:

$$F_L = -D_2 (n_x \nabla_z n_y - n_y \nabla_z n_x) \quad (14)$$

This term has in fact a Lifshitz-like structure, if we consider the layer normal \vec{v} , parallel to the z-axis:

$$F_L = -D_2 (\vec{n} \times \vec{v}) \cdot [\vec{v} (\vec{\nabla} \cdot \vec{n}) - (\vec{v} \cdot \vec{\nabla}) \vec{n}] = -D_2 (\vec{n} \times \vec{v}) \cdot [\vec{v} \text{div} \vec{n} + \vec{v} \times \text{rot} \vec{n}]. \quad (15)$$

We can identify this expression as a pseudoscalar inhomogeneous Dzyaloshinskii-Moriya interaction, which does not involve an external field but a fixed direction in the space, that is the vector \vec{v} normal to the smectic layer.

Chiral molecules can also form nematic phases called chiral nematic phases or cholesteric phases. The phase shows a nematic order, with the director rotating throughout the sample. The axis of this screw is normal to the director. The distance over which the director rotates by 2π is the chiral pitch, generally of the order of the wavelength of visible light.

If the nematic phase is composed of chiral molecules, all of the same chirality, the material does not have symmetry planes and then the free energy has, according to Landau and Lifshitz, a pseudoscalar term:

$$F_{chiral} = b \vec{n} \cdot \vec{\nabla} \times \vec{n}. \quad (16)$$

This is the pseudoscalar of the DM interaction as in Ref.4, and introduced in Sect.2. If we consider the vector \vec{v} as the direction of pitch, then the director \vec{n} lies in a plane perpendicular to it and then Equation 16 can be rewritten as:

$$F_{chiral} = b(\bar{n} \times \bar{v}) \cdot [\bar{v}(\bar{v} \cdot \bar{n}) - (\bar{v} \cdot \bar{v}) \cdot \bar{n}] \quad (17)$$

with the same structure that we encountered in the smectic term originating the helix.

6. The Saddle-Splay Elasticity at Surfaces

In nematics, a more general form of the distortion free-energy density, in the framework of the usual first-order continuum theory, is given as:

$$f = \frac{1}{2} K \left\{ (\text{div } \bar{n})^2 + (\bar{n} \cdot \text{rot } \bar{n})^2 + (\bar{n} \times \text{rot } \bar{n})^2 \right\} - (K + K_{24}) \text{div}[\bar{n} \text{ div } \bar{n} + \bar{n} \times \text{rot } \bar{n}] \quad (18)$$

where K is the bulk elastic constant in the case of elastic isotropy. The last term is the contribution of the saddle-splay elasticity. This contribution is not usually inserted in the bulk free energy, because it becomes a surface contribution when integration is performed on the cell thickness [25,26]. The saddle-splay contribution is then a Lifshitz invariant of the surface energy:

$$f_{surface} = -(K + K_{24}) \bar{v} \cdot [\bar{n} \text{ div } \bar{n} + \bar{n} \times \text{rot } \bar{n}] \quad (19)$$

if \bar{v} is the unit vector of direction perpendicular to the surface containing the nematic material. This term has the same form of Lifshitz scalar product in Equation 4.

In addition to the anchoring energy, which is the anisotropic part of surface tension, there is an elastic contribution, which has been originally indicated as a part of the bulk elastic energy in the form of a divergence [27-29]. This contribution can be viewed as the elastic part of surface energy depending on the tangential gradient of director. The K_{24} term may induce spontaneous twist deformations in hybrid nematic films with azimuthally degenerate anchoring conditions. Such deformations are manifested in the formation of periodic stripe domains observed in sufficiently thin hybrid NLC cells [25,30]. If the anchoring energy is sufficiently small, the Lifshitz term can produce a modulated-tilt state has recently shown by Lelidis and Barbero [31].

The saddle-splay contribution is necessary, when we have to evaluate the elastic contribution of thin films or membranes. In 1973, Helfrich studied the energetic cost of a generic sheet in a three-dimensional space: we can determine, in each point of the sheet, the radii of curvature r_1 and r_2 , and local curvatures $c_1 = 1/r_1$ and $c_2 = 1/r_2$. Curvatures can be positive or negative. Saddle-shaped surfaces have curvature that is positive along one principal axis and negative along the other. The energetic cost per unit area associated with bending a membrane, as noted by Helfrich [32], is given by the sum of two terms, one dependent on total curvature, $c_1 + c_2$, and the other on product $c_1 c_2$:

$$F_S = \frac{1}{2} k_C (c_1 + c_2 - 2c_0)^2 + k_G c_1 c_2 \quad (20)$$

In this expression, k_C is the bending (or curvature) modulus and k_G is the saddle-splay (or Gaussian curvature) modulus. These two modules are set by interactions among membrane molecules. The spontaneous curvature is denoted by c_0 . As reported in [33], biological membranes are sheets that can be modelled with a continuum elastic approach. These membranes are two-dimensional fluids within which proteins diffuse and interact. Membranes can bend and curve, with deformations

controlled by proteins and lipids; the converse is also true, it is the structure created by membrane curvature can guide the spatial organisation of membrane molecules. Then the membrane can display spatial patterning at length-scales far greater than the scale of individual molecules [33].

7. The Hybrid Cell and the Flexoelectricity

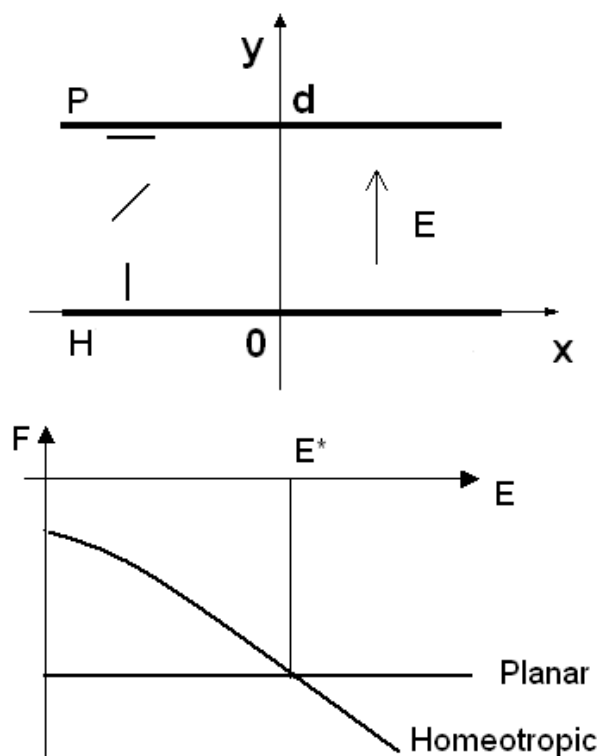
Let us start the discussion of some case studies. The first is on the role of flexoelectricity in hybrid nematic cells. A hybrid cell is a nematic cell where a sample is confined between two parallel walls with different anchoring conditions. One surface is treated to favour a planar alignment; the opposite one is favouring a homeotropic alignment. The cell is then named HAN, that is Hybrid Aligned Nematic cell. The hybrid cell we discuss has the y -axis perpendicular to cell walls (see the upper part of Figure 3).

An electric field can be applied parallel to y -axis: we have then $\vec{E} = E\vec{j}$ where \vec{j} is the unit vector of y -axis. \vec{j} is the homeotropic direction too. The unit vector \vec{i} , parallel to the cell walls, gives the easy planar direction. The bulk free energy density is given, in the elastic isotropic approximation, by:

$$f_{Bulk} = \frac{1}{2} K \left[(\text{div } \vec{n})^2 + (\text{rot } \vec{n})^2 \right] - \frac{\epsilon_o \Delta \epsilon}{2} (\vec{E} \cdot \vec{n})^2 \quad (21)$$

where the last term is due to the dielectric anisotropy $\Delta \epsilon$ of the nematic.

Figure 3. Frame of reference for the hybrid cell in the upper part of the figure. In the lower part, the free energies as a function of the electric field, in the case of planar and homeotropic configurations. Note the presence of a threshold.



The surface energy in the Rapini-Papoular form can be used:

$$f_{Surf} = \left[W_P (\vec{n} \cdot \vec{i})^2 - W_H (\vec{n} \cdot \vec{j})^2 \right] \quad (22)$$

at the two surfaces, for $y=d$ and for $y=0$. W_P, W_H are energy densities of the surface anchoring. If we have a planar cell with surface S , thickness d , and a uniform director configuration $\vec{n} = n \vec{i}$, the total free energy is $F_{Planar} = -2S W_P$. If the director configuration is uniform but homeotropic, then $\vec{n} = n \vec{j}$ and the total free energy is the sum of the energy due to the presence of electric field and surfaces: $F_{Hom} = -\epsilon_o \Delta \epsilon E^2 / 2 - 2S W_H$.

When $W_P, W_H > 0$, we have a homeotropic cell; if $W_P, W_H < 0$ the cell is planar. Graphically comparing (lower part of Figure 3) the energies of the homeotropic and planar cells, we see the possibility of an electric threshold field E^* : under this value of the electric field, it is favoured the planar configuration, over the threshold value, it is the homeotropic configuration that has a lower energy.

In a hybrid cell, the director changes from a planar configuration at one of the cell wall, to a homeotropic configuration at the other cell wall. The tilt angle is then depending on y , as a function $\theta = \theta(y)$. The director field is given by: $\vec{n} = \cos \theta \vec{i} + \sin \theta \vec{j}$.

If the anchoring is strong, the tilt angle is $\theta = \pi/2$ at $y=0$ - homeotropic wall, and $\theta = 0$ at $y=d$ - planar wall. In the one elastic constant approximation, we have the bulk free energy density in the form:

$$f_{Bulk} = \frac{K}{2} \left(\frac{\partial \theta}{\partial y} \right)^2 - \frac{\epsilon_o \Delta \epsilon}{2} E^2 \sin^2 \theta \quad (23)$$

and the surface energy density $f_{Surf} = -W_P - W_H$. To represent a hybrid configuration in a very rough approach, let us simply choose a linear function of the tilt angle with y . Then:

$$\theta = -\frac{\pi}{2} \frac{y}{d} + \frac{\pi}{2} \quad (24)$$

with $\theta_o = \pi/2$ and $\theta_d = 0$. Then $\partial \theta / \partial y = -\pi/2d$ and the total bulk energy is:

$$F_{Bulk} = S \int_0^d \frac{K}{2} \left(\frac{\partial \theta}{\partial y} \right)^2 dy - \frac{\epsilon_o \Delta \epsilon}{2} E^2 S \int_0^d \sin^2 \theta dy = \frac{K \pi^2 S}{8d} - \frac{\epsilon_o \Delta \epsilon}{4} E^2 S d \quad (25)$$

Including the surface energy, the total energy is:

$$F_{Tot} = \frac{K \pi^2 S}{8d} - \frac{\epsilon_o \Delta \epsilon}{4} E^2 S d - S (W_P - W_H) \quad (26)$$

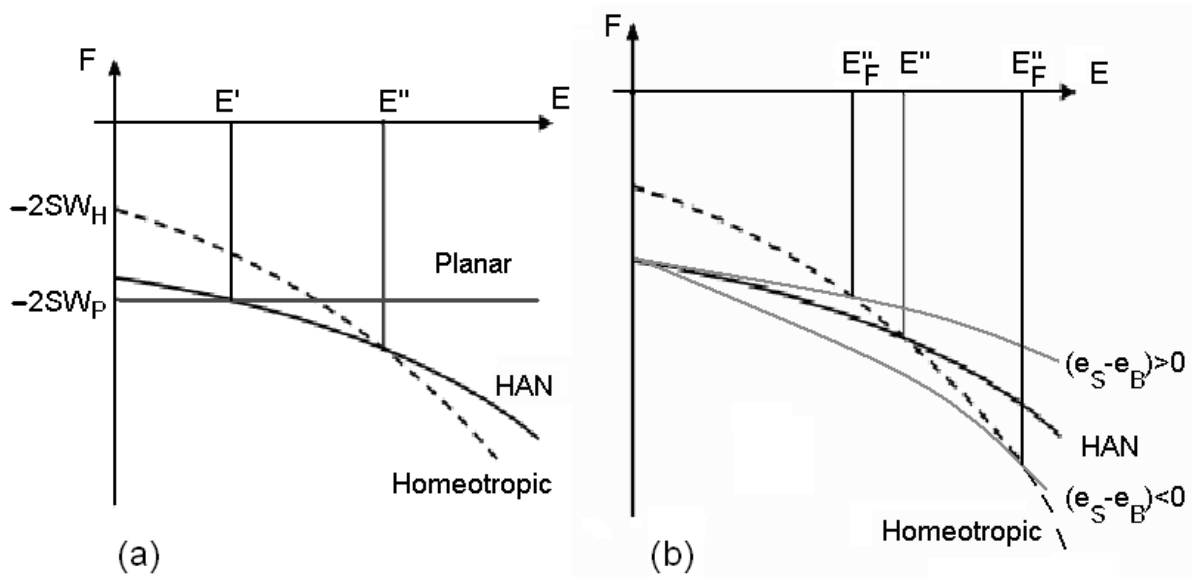
Let us compare this expression with the energy of the cell in homeotropic and planar configurations, choosing an anchoring energy favouring planar and hybrid configurations under threshold fields:

$$F_{Planar} = -2S W_P \quad ; \quad F_{Homeotropic} = -\frac{\epsilon_o \Delta \epsilon}{2} E^2 S d - 2S W_H \quad (27)$$

$$F_{Hybrid} = \frac{K\pi^2 S}{8d} - \frac{\epsilon_0 \Delta \epsilon}{4} E^2 S d - S(W_P - W_H) \tag{28}$$

What is shown in Figure 4(a) is surely possible, because we can adjust the anchoring parameters. We observe then two threshold fields: when the field is lower than E' , the nematic is planar, if the field is comprised between E' and E'' , the cell is hybrid. Over E'' , the cell is homeotropic.

Figure 4. (a) Behaviour of the free energies of planar, hybrid (HAN) and homeotropic configurations, as functions of the electric field. Note the existence of two thresholds for the transition between the planar and the HAN configuration and between the HAN and the homeotropic configuration. (b) The two curves in grey show how the energy of the HAN configuration changes for the presence of flexoelectricity. According to the sign of the flexoelectric parameter, the threshold field is raised or lowered.



As previously discussed, the electric field can be coupled with a polarization arising from an elastic deformation in the flexoelectric effect. In planar and homeotropic configurations, because there are not deformations of director, the flexoelectric effect is absent, but in the hybrid cell the deformation gives a flexoelectric polarization $\vec{P} = (e_S \vec{n} \text{div } \vec{n} + e_B \vec{n} \times \text{rot } \vec{n})$, different from zero. Previous investigations on the role of this polarization can be found in Ref. 34.

Let us add the term $f_{Flexo} = -\vec{P} \cdot \vec{E}$ to the free energy density, which is:

$$f_{Flexo} = -\vec{P} \cdot \vec{E} = -(e_S - e_B) E \sin\theta \cos\theta \frac{\partial\theta}{\partial y} \tag{29}$$

If θ is given by Equation (24), after integrating on the cell volume, we have the contribution of flexoelectricity to the total free energy as:

$$F_{flexo} = -(e_S - e_B) E S \tag{30}$$

In principle, the coefficient $(e_S - e_B)$ could be positive or negative, depending on the value of splay and bend parameters. The threshold values E', E'' are changed from the contribution of the

flexoelectricity. They could be lowered or raised by the induced polarization (see Figure 4(b)). The thresholds change according to the shape of the molecules. Comparing the thresholds we can estimate the values of the coefficients. The two electric field contributions in the HAN cell are:

$$F_1 = - \frac{\varepsilon_o \Delta \varepsilon}{4} E^2 S d ; F_2 = - (e_S - e_B) E S \quad (31)$$

If they were of the same order of magnitude, we could obtain:

$$(e_S - e_B) \approx \frac{\varepsilon_o \Delta \varepsilon}{4} E d \quad (32)$$

In the case of a cell with a thickness of $10 \mu m$, a field of $10 V/\mu m$, and an electric anisotropy as $\Delta \varepsilon = 0.1$ we obtain:

$$(e_S - e_B) \approx 25 \frac{pC}{m} \quad (33)$$

in agreement with Ref.35 and with other experimental values [36-40]. Recently a giant flexoelectricity has been found with bent-core nematics: a peak of $35 nC/m$ was measured in these materials then more than 3 orders of magnitude larger than in calamitics [41]. In the next section we will study the alignment transitions in the nematic cells; such a problem was studied also in Ref.42.

8. The Phase Diagrams of the Hybrid Cell

Let us consider the hybrid cell as in the previous section. We use the same notation here but we solve the Euler-Lagrange equation with the proper boundary conditions, by means of an iterative procedure previously used in Ref.43, to investigate the ion densities in corona plasma. The Euler-Lagrange equation is:

$$\frac{\partial f_{Bulk}}{\partial \theta} = \frac{\partial}{\partial y} \frac{\partial f_{Bulk}}{\partial (\partial \theta / \partial y)} \quad (34)$$

and:

$$f_{Bulk} = \frac{K}{2} \left(\frac{\partial \theta}{\partial y} \right)^2 - \frac{\varepsilon_o \Delta \varepsilon}{2} (E \sin \theta)^2 \quad (35)$$

that is:

$$\frac{\partial^2 \theta}{\partial y^2} + \zeta^2 \sin \theta \cos \theta = 0 \quad ; \quad \zeta^2 = \varepsilon_o \Delta \varepsilon E^2 / K \quad (36)$$

and the surface energy density:

$$f_{surf} = - W_H \sin^2 \theta_o + W_P \sin^2 \theta_d \quad (37)$$

where $W_H > 0$ and $W_P < 0$. The boundary conditions are given by the following equations:

$$-K \left(\frac{\partial \theta}{\partial y} \right)_{y=0} = |W_H| (\sin 2\theta)_{y=0} \quad ; \quad -K \left(\frac{\partial \theta}{\partial y} \right)_{y=d} = |W_P| (\sin 2\theta)_{y=d} \quad (38)$$

Equation 36 can be rigorously solved with elliptic functions: in Ref.44, the existence of a critical thickness for a hybrid aligned nematic cell was predicted in the framework of a rigorous solution. Nevertheless, numerical solutions and an approximate analytic theory have been already used, when studying the existence of flexoelectric instabilities in the case of asymmetric boundary conditions [45]. Here, we use an approximate solution to the non-linear problem of the form:

$$\theta = \theta^o(y) + \theta'(y) \quad (39)$$

and then Equation 36 can be written as two equations:

$$\frac{\partial^2 \theta^o}{\partial y^2} = 0 \quad ; \quad \frac{\partial^2 \theta'}{\partial y^2} = -\xi^2 \sin 2\theta^o \quad (40)$$

The second equation in (40) is solved in the following iteration:

$$\frac{\partial^2 \theta^{j+1}}{\partial y^2} = -\xi^2 \sin 2\tilde{\theta}^j \quad (41)$$

where $\tilde{\theta}^j = \theta^o + \theta^j$ and $\tilde{\theta}^o = \theta^o$. Three steps of the iteration are enough to have the solution within 0.1 %. Then $\theta = \theta^o(y) + \theta^{j+1}(y)$, where:

$$\theta^o(y) = \alpha_o + \alpha_1 y \quad ; \quad \theta^{j+1}(y) = -\xi^2 \int_0^y \int_0^{y'} \sin 2\tilde{\theta}^j(y') dy' dy'' \quad (42)$$

The boundary conditions are:

$$d \left(\frac{\partial \theta}{\partial y} \right)_{y=0} + b_o (\sin 2\theta)_{y=0} = 0 \quad ; \quad d \left(\frac{\partial \theta}{\partial y} \right)_{y=d} + b_1 (\sin 2\theta)_{y=d} = 0 \quad (43)$$

in which we used the dimensionless parameters $|W_H d / K| = b_o$; $|W_P d / K| = b_1$. From the first equation in the boundary conditions (43):

$$\alpha_1 d + b_o (\sin 2\alpha_o) = 0 \quad (44)$$

Once we chose the value of α_o , from Equation (44), we have the value of α_1 , and then, after iteration, the solution $\theta = \theta^o + \theta'$. To determine the value of α_o we could use the other boundary condition, the second in (43); but, in this case, we are facing a strongly oscillating function. It is better to determine the value of parameter α_o , minimizing the total free energy. Adding the flexoelectricity, the term to include in the free energy density is:

$$f_{Flexo} = -(e_S - e_B) E \sin \theta \cos \theta \frac{\partial \theta}{\partial y} \quad (45)$$

and, after integration on the cell thickness, we have a further contribution to the surface energy density of the form:

$$F_{Flexo} = -(e_S - e_B)E[\sin \theta_o - \sin \theta_d]. \tag{46}$$

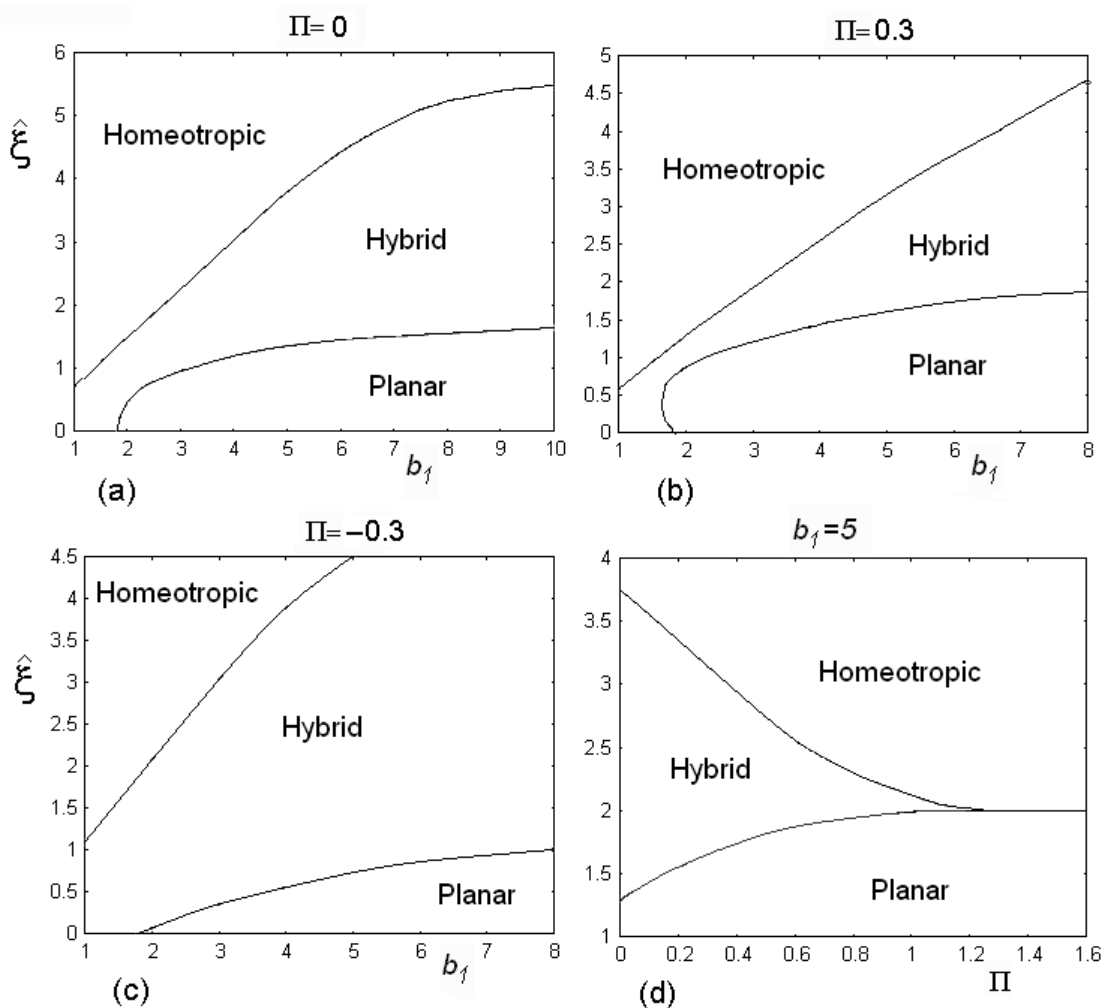
This term can be easily inserted in the numerical calculation, to minimize the total free energy. Let us introduce the following dimensionless variables and parameter:

$$\hat{y} = \frac{y}{d}; \hat{\xi} = \xi d; \Pi = (e_S - e_B) \sqrt{\frac{2}{K\epsilon_o \Delta \epsilon}} \tag{47}$$

to illustrate the results of calculations.

In Figure 5 we can see the phase diagrams of the HAN cell, for a fixed choice of the surface parameter $b_o = 1$. We can change the value of parameter b_1 and find the value of the threshold field (the electric field is dimensionless represented by $\hat{\xi}$).

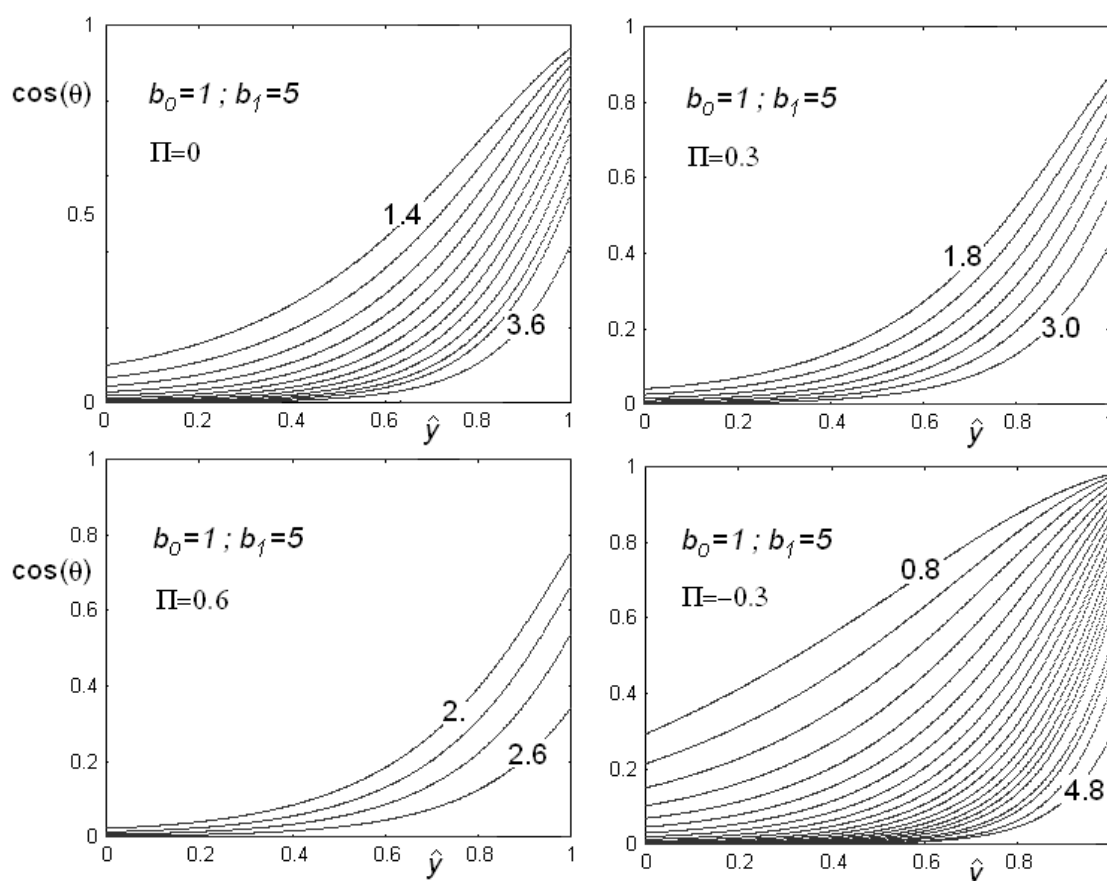
Figure 5. Phase diagrams of the HAN cell, for a fixed choice of the surface parameter $b_o = 1$. We change the value of parameter b_1 and find the value of the thresholds of the electric dimensionless field $\hat{\xi}$. There are three regions in the diagrams where planar, homeotropic and hybrid alignments are allowed. The phase diagram is depending on the values of flexoelectric parameter Π . Diagram (d) shows the behaviour of a cell when the flexoelectric parameter Π changes. Note that the hybrid configuration disappears when flexoelectric parameter is higher than 1.3.



There are three regions in the diagrams where planar, homeotropic and hybrid alignments are allowed according to the values of the electric field. The phase diagram is depending on the values of flexoelectric parameter Π (see diagrams (a),(b) and (c) in Figure 5). The last diagram (d) shows the behaviour of a cell when we change the flexoelectric parameter Π . Note that the hybrid configuration disappears when flexoelectric parameter is higher than value 1.3.

In Figure 6, we see the behaviour of $\cos \theta$ as a function of the dimensionless variable $\hat{y} = y/d$ in the case of positive and negative flexoelectric coefficients, for different values of the electric field. Note that, as the field increases, the role of surface is suppressed and the angle at the planar surface increases. As the electric field is higher than the threshold value, the cell becomes homeotropic and $\cos \theta = 0$.

Figure 6. Behaviour of $\cos \theta$ as a function of the reduced cell thickness $\hat{y} = y/d$ in the case of positive and negative flexoelectric coefficients, for different values of the dimensionless electric field (some values are reported on the curves). Note that, as the field increases, the role of surface is suppressed and the angle at the planar surface increases. As the electric field is higher that the threshold value, the cell becomes homeotropic and then $\cos \theta = 0$.



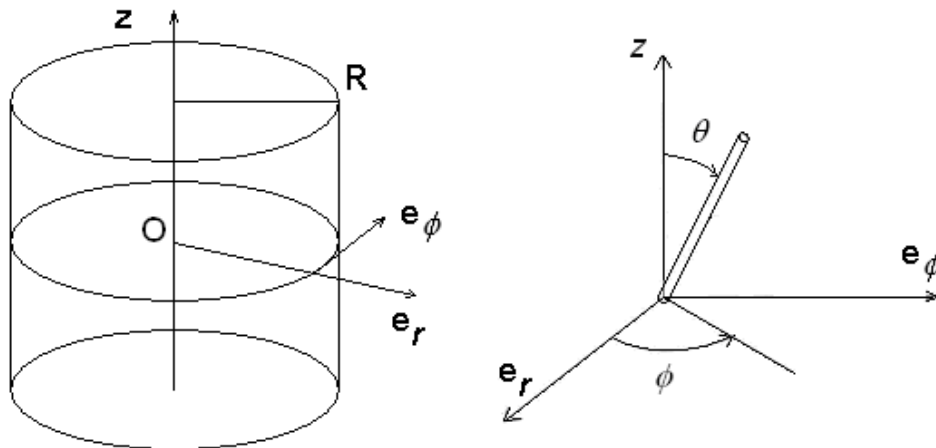
To conclude this section on HAN cells, let us remember that we have another Lifshitz invariant, that gives the saddle-splay contribution to the surface free energy density, in the form: $f_{Saddle-splay} = -(K + K_{24}) \vec{v} \cdot [\vec{n} \text{div} \vec{n} + \vec{n} \times \text{rot} \vec{n}]$. In the hybrid cell alignment, where only the tilt angle is displayed by the elastic distortion, this contribution is zero. We will see in the last section of the

paper, how this term produces a periodic distortion and how the PHAN - the Periodic HAN - texture appears. The fact that the saddle-splay contribution is zero in the HAN configuration, is in agreement with the conclusion that in the same configuration the flexoelectric contribution $f_{Flexo} = -\vec{E} \cdot [e_S \vec{n} \operatorname{div} \vec{n} + e_B \vec{n} \times \operatorname{rot} \vec{n}]$ is zero too, when $e_S = e_B$. As we saw in Sect.4, it is the periodic distortion to origin a contribution different from zero, if $e_S \neq e_B$.

9. Nematics in Cylindrical Geometry

Let us consider a cylinder with radius R . In this cylindrical cell we imagine to insert a nematic. We use the frame as in Figure 7 and solve the Euler-Lagrange equation in cylindrical coordinates.

Figure 7. Cylindrical cell and frame of references on the left and on the right the angles of director chosen for calculations.



Let us consider $\theta = \theta(r)$, only depending on the radial distance, and moreover, $\phi = 0$. The Euler-Lagrange is:

$$\frac{\partial f_{Bulk}}{\partial \theta} = \frac{1}{r} \frac{\partial}{\partial r} \left(r \frac{\partial f_{Bulk}}{\partial (\partial \theta / \partial r)} \right) \tag{48}$$

The bulk density energy is given by:

$$f_{Bulk} = \frac{K}{2} \left[\left(\frac{\partial \theta}{\partial r} \right)^2 + \frac{\sin^2 \theta}{r^2} + 2 \frac{\sin \theta \cos \theta}{r} \left(\frac{\partial \theta}{\partial r} \right) \right] - \frac{\epsilon_o \Delta \epsilon}{2} (E \cos \theta)^2 \tag{49}$$

and then the Euler-Lagrange equation turns out to be:

$$\frac{\sin \theta \cos \theta}{r^2} + \zeta^2 \sin \theta \cos \theta = \frac{1}{r} \frac{\partial}{\partial r} \left(r \frac{\partial \theta}{\partial r} \right) ; \quad \zeta^2 = \epsilon_o \Delta \epsilon E^2 / K \tag{50}$$

The surface energy density is:

$$f_{Surf} = -W_H \sin^2 \theta_R + W_P \sin^2 \theta_R \tag{51}$$

where $W_H > 0$; $W_P < 0$. For an anchoring, which favours an homeotropic alignment of the nematic perpendicular at the wall of the cylinder, we use:

$$f_{Surf} = -W_H \sin^2 \theta_R \quad (52)$$

If we want to avoid the presence of a defect at the axis of cylinder (z – axis), the director must escape in the z – direction. The solution, if the applied electric field is zero, is given by an inverse tangent:

$$\theta^o(r) = 2 \tan^{-1} \left(\beta \frac{r}{R} \right) \quad (53)$$

where $\beta = 1$, for a strong anchoring at the cylinder wall. This is a well-know solution due to Belavin and Polyakov [46]. To solve the equation in the case of electric field different from zero, we choose a solution as:

$$\theta(r) = \theta^o(r) + \theta'(r) \quad (54)$$

The use of an approximate solution could be questionable. Nevertheless, linearization and approximation of Belavin-Polyakov equation are reported in the literature [45,47]. Using (54), we have two equations to solve:

$$\begin{aligned} \frac{\sin \theta^o \cos \theta^o}{r^2} &= \frac{1}{r} \frac{\partial}{\partial r} \left(r \frac{\partial \theta^o}{\partial r} \right) \\ \zeta^2 \sin \theta^o \cos \theta^o &= \frac{1}{r} \frac{\partial}{\partial r} \left(r \frac{\partial \theta'}{\partial r} \right) \end{aligned} \quad (55)$$

The second equation can be solved with iterations. At the fourth step of iteration the solution is within 0.1%. In the following way, we have:

$$\zeta^2 \sin \tilde{\theta}^j \cos \tilde{\theta}^j = \frac{1}{r} \frac{\partial}{\partial r} \left(r \frac{\partial \theta^{j+1}}{\partial r} \right) \quad ; \quad \tilde{\theta}^j = \theta^o + \theta^j \quad (56)$$

Actually, we arrive at the following solutions:

$$\theta^o(r) = 2 \tan^{-1} \left(\beta \frac{r}{R} \right) \quad ; \quad \theta^{j+1}(r) = \zeta^2 \int_0^r \frac{dr''}{r''} \int_0^{r''} \sin \tilde{\theta}^j(r') \cos \tilde{\theta}^j(r') r' dr' \quad (57)$$

and then at final solution $\theta(r) = \theta^o(r) + \theta^{j+1}(r)$. To determine the value of parameter β we choose the solution minimizing a reduced total free energy:

$$\frac{F_{Bulk}}{2\pi RL} = \int_0^d f_{Bulk} r dr + f_{Surf} \quad (58)$$

where L is an arbitrary length of the cylindrical cell.

Let us then consider the contribution of flexoelectricity to Euler-Lagrange equations:

$$\frac{\partial f_{Flexo}}{\partial \theta} - \frac{1}{r} \frac{\partial}{\partial r} \left(r \frac{\partial f_{Flexo}}{\partial (\partial \theta / \partial r)} \right) = (e_S - e_B) E \frac{\sin^2 \theta}{r} \tag{59}$$

We use again $(e_S - e_B) E = \Pi \xi$ and $b = WR/K$ as parameters. The equation to solve is:

$$\xi^2 \sin \tilde{\theta}^j \cos \tilde{\theta}^{j+1} + \Pi \xi \frac{\sin^2 \tilde{\theta}^j}{r} = \frac{1}{r} \frac{\partial}{\partial r} \left(r \frac{\partial \theta^{j+1}}{\partial r} \right) \tag{60}$$

instead of Equation (56). Figures 8 and 9 show the results of calculations for different values of anchoring and flexoelectric coefficients. In the Figure 8 we can see the angle θ as a function of the reduced radial distance r/R , for two values of the flexoelectric coefficient, $\Pi = 0$ and 1. The figure shows the behaviour in the case of different values of anchoring parameter b and of dimensionless electric field parameter $\xi = \xi R$. As the electric field is higher than a threshold value, angle θ goes to zero and the director field is parallel to cylinder axis in all the cell. The following Figure 9 shows $\cos \theta$ as a function of reduced radial distance r/R , for different values of Π and ξ . In this case, the value of the anchoring strength is fixed. Note that a negative value of the flexoelectric parameter is strongly favouring the alignment of the director parallel to cylinder axis, and then we find a low value of the threshold electric field. If flexoelectric parameter Π is positive and large, the distorted configuration is favoured, and the threshold field required for suppressing this configuration is increased. Moreover, if the flexoelectric parameter is large, as in the lower image in Figure 9, angle θ starts to oscillate as the field increases. We must have a huge electric field to suppress the oscillating distortion and have $\cos \theta = 0$, with all the nematic aligned parallel to the field, in a uniform configuration.

In Figure 10, the phase diagrams are shown, when anchoring parameter b is fixed and equal to 6. We see three regions, denoted by: U for uniform alignment of director parallel to z-axis, D if the director has a deformed configuration, and O when the director is oscillating and cosine becomes negative too. Angle θ turns more than $\pi/2$ on the distance R . As told before, giant flexoelectric coefficients are possible and then the oscillation could be experimentally tested in cylindrical cells.

A last note on the flexoelectric term. The flexoelectric vector is a sum of two contributions:

$$\begin{aligned} \vec{P} &= (e_S \vec{n} \operatorname{div} \vec{n} + e_B \vec{n} \times \operatorname{rot} \vec{n}) = \\ &= e_S D (\sin \theta \vec{u}_r + \cos \theta \vec{u}_z) + e_B R (-\cos \theta \vec{u}_r + \sin \theta \vec{u}_z) = e_S D \vec{n} + e_B R \vec{t} \end{aligned} \tag{61}$$

where $D = \operatorname{div} \vec{n}$, $R = (\operatorname{rot} \vec{n})_\varphi$. These two components which are perpendicular each other: when they are coupled with the electric field, parallel to the cylinder axis, we have then the two contributions in bulk energy with an opposite sign.

To conclude this section, let us discuss the saddle-splay contribution to the free energy, that is:

$$f_{Saddle-splay} = -(K + K_{24}) \operatorname{div} [\vec{n} \operatorname{div} \vec{n} + \vec{n} \times \operatorname{rot} \vec{n}] \tag{62}$$

In the previous assumptions, $\theta = \theta(r), \varphi = 0$, $f_{Saddle-splay}$ is simply renormalizing the value of the surface energy and then we do not further discuss it.

Figure 8. Behaviour of θ as a function of the reduced radial coordinate r/R in the case of flexoelectric coefficient Π equal to 0 and 1, for different values of the anchoring parameter b and dimensionless electric field (some values are reported on the curves). As the electric field is higher than a threshold value, angle θ goes to zero, that is the director field is parallel to the cylinder axis.

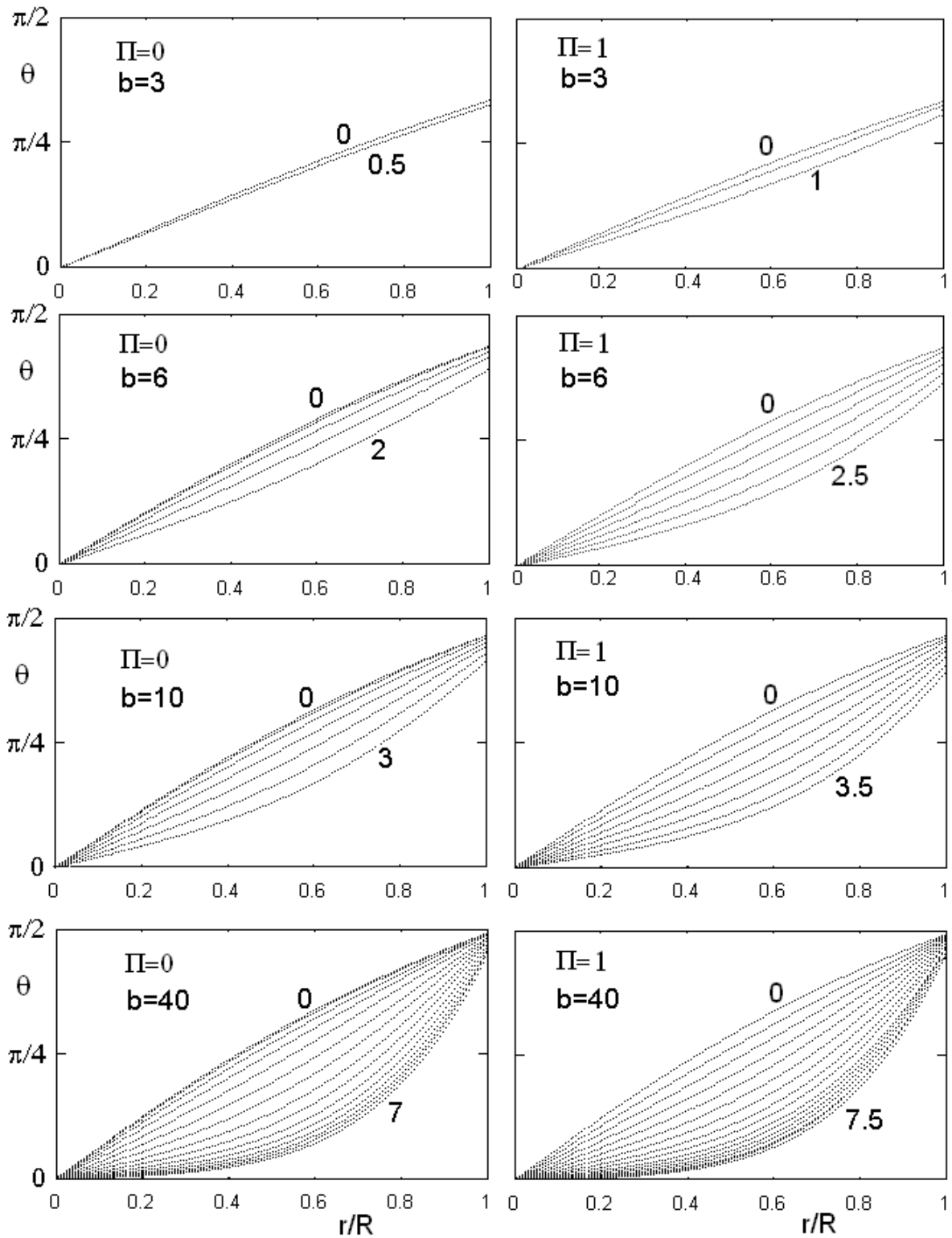


Figure 9. Behaviour of $\cos\theta$ as a function of the reduced radial coordinate r/R , for different values of the flexoelectric coefficient Π and of the dimensionless electric field (some values of $\hat{\xi}$ are reported on the curves). The value of the anchoring strength is fixed in all the figures. Note that a negative value of the flexoelectric parameter is strongly favouring the alignment of director parallel to cylinder axis, and then the threshold electric field is very low. If the flexoelectric parameter is positive and large, the distorted configuration is favoured, and the threshold field, needed for suppressing this configuration, is increased. As shown in the lower part of the figure, when Π is very large, $\cos\theta$ is oscillating as the electric field increases. A very large field is required to suppress the distortion and have $\theta = 0$.

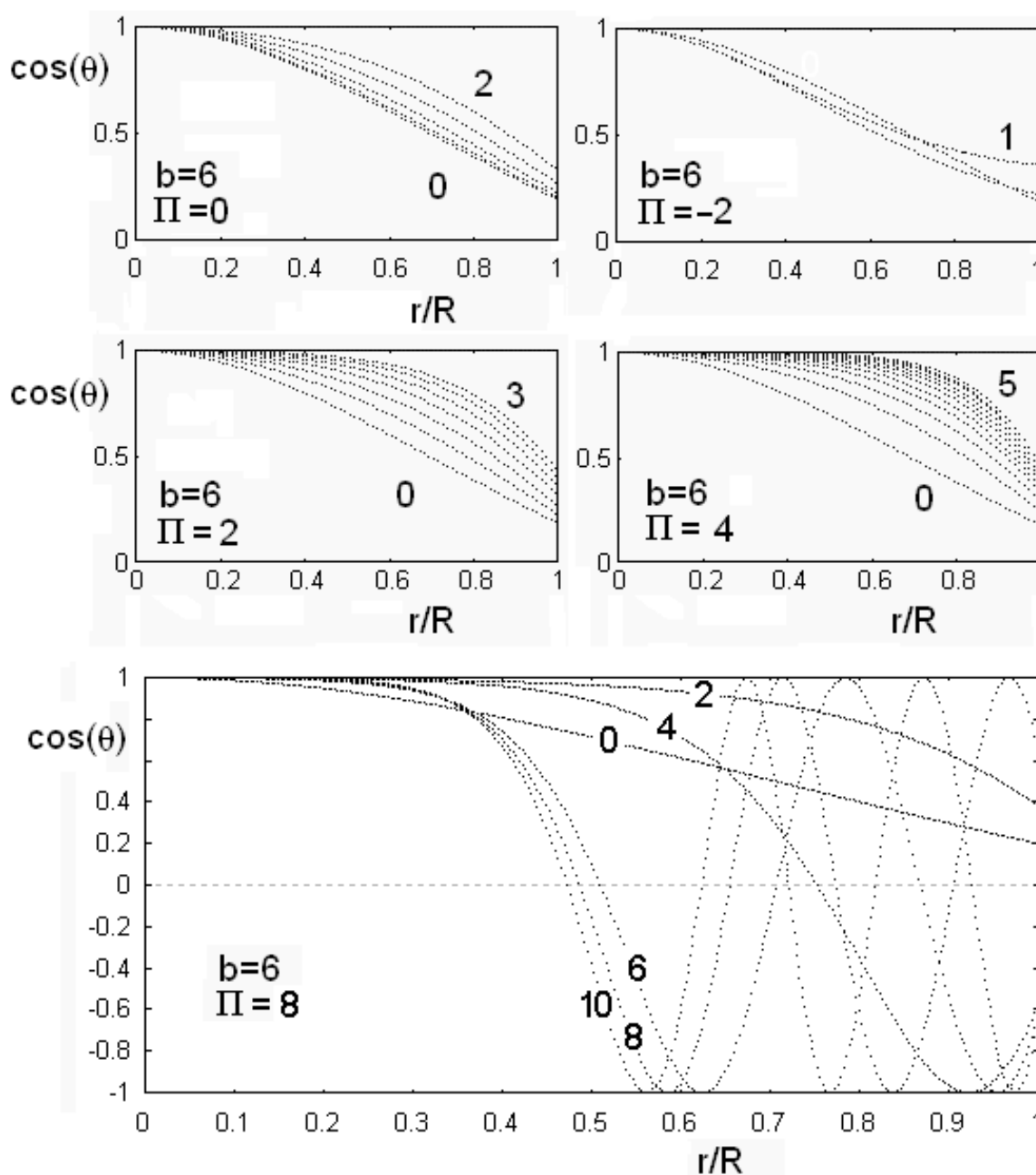
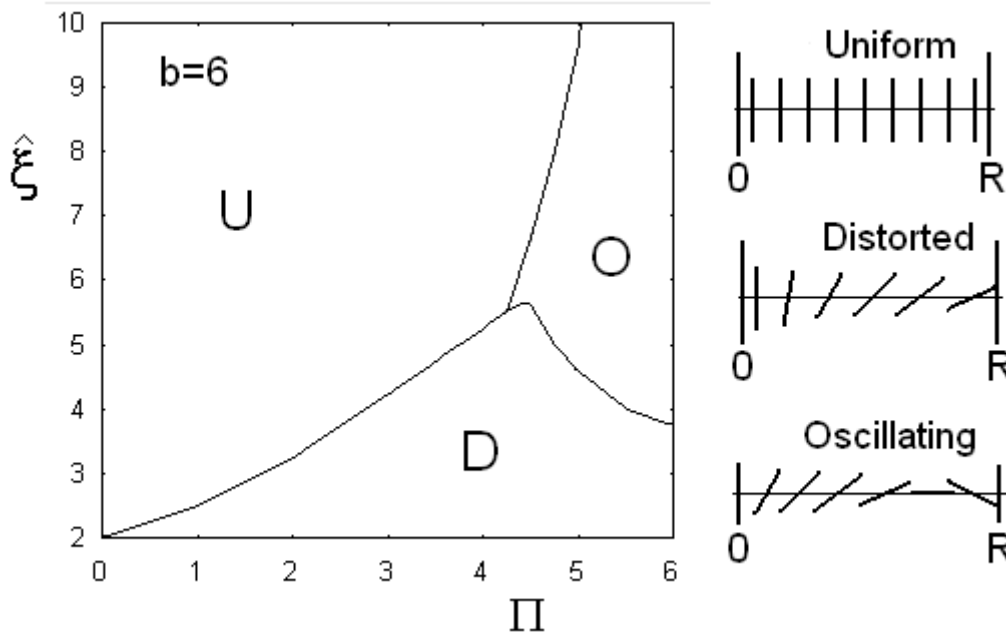


Figure 10. Phase diagram of the cylindrical confinement, when the anchoring parameter b is fixed and equal to 6. The three regions are denoted by U for the uniform alignment of director parallel to the cylinder axis, D when the director has a deformed configuration, and O if director is oscillating and cosine becomes negative too.



10. The Saddle-Splay Contribution and the PHAN Cell

Sometimes, it is possible to note a periodicity in the HAN cells observed by the polarised light microscope. Because of this periodic configuration, the cell is in the PHAN configuration, that is a nematic cell with a period hybrid alignment. Two angles describe the PHAN configuration: θ and φ . The last angle is formed by the projection of the director in the plane of the cell with the x -axis.

The free energy density is that by Nehring and Saupe, and given by Equation (19). The frame of reference is $[xyz]$, with $[xy]$ the cell plane and z -axis perpendicular to the cell plane. The homeotropic wall is at $z_0 = 0$, where z is the axis perpendicular to the cell plane. The planar wall is at $z_l = d$, where d is the thickness of the cell. The easy-axis of the planar alignment is chosen coincident with the x -axis. The director \vec{n} is described as:

$$\vec{n} = \vec{i} \cos \varphi \cos \theta + \vec{j} \sin \varphi \cos \theta + \vec{k} \sin \theta \tag{63}$$

The Euler-Lagrange equations are non-linear. They were solved in Ref.25, with a numerical approach to determine the threshold thickness of the cell between the planar and the PHAN. Here, we want to grasp the role of the saddle-splay contribution, with just simple calculations. Let us then consider the tilt angle θ depending on z , and the φ angle depending on x , in the following way:

$$\theta(z) = \frac{\pi z}{2d} \quad ; \quad \varphi(x) = \frac{2\pi x}{\Lambda} \tag{64}$$

The tilt is zero if $z = 0$, and it is $\pi/2$ at $z = d$. With Λ we denote the wavelength along x -axis. The free energy density is:

$$f_{Elastic} = \frac{K}{2} \left[\left(\frac{\pi}{2d} \right)^2 + \left(\frac{2\pi}{\Lambda} \right)^2 \sin^2 \varphi - \frac{2\pi^2}{\Lambda d} \cos^2 \theta \sin \varphi \right] \quad (65)$$

Let us integrate on the volume $V = d\Lambda D$, where D is a fixed distance on y – axis. We have:

$$F_{Elastic} = \frac{K}{2} \Lambda D d \left[\left(\frac{\pi}{2d} \right)^2 + \frac{1}{2} \left(\frac{2\pi}{\Lambda} \right)^2 \right] \quad (66)$$

Neglecting the anchoring with respect to φ , and assuming just tilt anchoring, with a surface energy density of the form:

$$f_{Surf} = -W n_z^2 \quad (67)$$

where $W = W_P$ for planar anchoring with $\theta = 0$, and $W = W_H$ at the homeotropic anchoring $\theta = \pi/2$. After integrating on surfaces of the cell:

$$F_{Surf} = - (W_P + W_H) \Lambda D \quad (68)$$

and then the total free energy is:

$$F = \frac{K}{2} \Lambda D d \left[\left(\frac{\pi}{2d} \right)^2 + \frac{1}{2} \left(\frac{2\pi}{\Lambda} \right)^2 \right] - (W_P + W_H) \Lambda D \quad (69)$$

Let us evaluate the saddle-splay contribution to free energy density, using Equation 4 of Ref.25, that here reduces to:

$$f_{Saddle-splay} = 2(1 + \kappa_4)K \left[-\theta_H \left(\frac{\partial \varphi}{\partial x} \right)_H \right] = 2(1 + \kappa_4)K \left[-\frac{\pi}{2} \frac{2\pi}{\Lambda} \right] \quad (70)$$

where $\kappa_4 = K_{24}/K$; after integration on a surface $S = \Lambda D$, we have:

$$F_{Saddle-splay} = -2(1 + \kappa_4)K\pi^2 D \quad (71)$$

The total energy is then:

$$F_{PHAN} = \frac{K\pi^2 D\Lambda}{8d} + \frac{K\pi^2 d D}{\Lambda} - (W_P + W_H)\Lambda D - 2(1 + \kappa_4)K\pi^2 D \quad (72)$$

Comparing with the free energy of HAN configuration:

$$F_{PHAN} \approx F_{HAN} \quad (73)$$

and after simple calculations we find:

$$d^2 - 2(1 + \kappa_4)\Lambda d - \frac{1}{8} \Lambda^2 = 0 \quad (74)$$

Neglecting the last term, we find a threshold value for the cell thickness:

$$d_c \cong 2\Lambda(1 + \kappa_4) \quad (75)$$

If $d > d_c$, then we find a HAN configuration, but if $d < d_c$ the modulated PHAN texture is displayed in the cell. In Ref.25, we can see the experimental observation of thickness threshold in a nematic sample. This is just a rough discussion on the role of saddle-splay contribution in producing periodic instabilities, but enough to understand the origin of a threshold thickness in the sample.

Let us remember that $f_{Saddle-splay} = -(K + K_{24}) \vec{v} \cdot [\vec{n} \operatorname{div} \vec{n} + \vec{n} \times \operatorname{rot} \vec{n}]$ is a Lifshitz invariant, with the same structure of flexoelectric contribution $f_{flexo} = -\vec{E} \cdot [e_S \vec{n} \operatorname{div} \vec{n} + e_B \vec{n} \times \operatorname{rot} \vec{n}]$ when $e_S = e_B$. We could imagine a surface contribution of the form $f_{Saddle-splay} = -\vec{v} \cdot [c_S \vec{n} \operatorname{div} \vec{n} + c_B \vec{n} \times \operatorname{rot} \vec{n}]$, where coefficients are different. This could increase the variety of observable configurations.

11. Conclusions

This paper is divided in two parts. In the first we have discussed the analogies among Lifshitz invariants in magnetic materials and liquid crystals. We saw that the structure of these invariants is the same, and that they are producing periodic instabilities in both cases. In the Lifshitz invariant, the interaction is between an external action and the order parameter, in a form that contains the gradient of order parameter. The external action can be an electric field applied to the bulk, and in this case the relevant effect is the flexoelectricity, or the confinement due to free surfaces or cell walls. The Lifshitz invariant related to surfaces gives the saddle-splay contribution to surface energy.

In the second part of the paper we discussed in depth the role of flexoelectricity in the case of confined nematics. We performed detailed calculations in the case of planar and cylindrical geometry. Phase diagrams are also shown, to see the alignment phase transitions due to electric field and the role of flexoelectric parameter.

References

1. Landau, L.D.; Lifshitz, E.M. *Statistical Physics*; Pergamon Press: Oxford, UK, 1980.
2. Braginsky, A.Y. Phenomenological theory of phase transitions to a state with irregular phase of the order parameter. *Phys. Rev. B* **2002**, *66*, 054202:1-054202:8.
3. Dzyaloshinskii, I.E. Theory of helicoidal structures in antiferromagnets. *Sov. Phys. JETP* **1964**, *19*, 960-971.
4. Bogdanov, A.N.; Rössler, U.K.; Pfleiderer C. Modulated and localized structures in cubic helimagnets. *Physica B* **2005**, *259-361*, 1162-1164.
5. Kadomtseva, A.M.; Popov, Yu.F.; Vorob'ev, G.P.; Ivanov, V.Yu.; Mukhin, A.A.; Balbashov, A.M. Specific features of the magnetic field-induced orientational transition in EuMnO_3 . *JETP Letters* **2005**, *81*, 590-593.
6. Dozov, I. On the spontaneous symmetry breaking in the mesophases of achiral banana-shaped molecules. *Europhys. Lett.* **2001**, *56*, 247-253.
7. Sarkissian, H.; Park, J.B.; Zeldovich, B.Ya.; Tabirian, N.V. Liquid crystal structure with transverse periodic alignment. Quantum Electronics and Laser Science Conference, QELS '05; Baltimore, Maryland, USA, May 22, 2005; Volume 3, pp. 1597-1599.
8. Marinova, Y.; Kosmopoulos, J.; Weissflog, W.; Petrov, A.G.; Photinos, D.J. Flexoelectricity of wedge-like molecules in nematic mixtures. *Mol. Cryst. Liquid Cryst.* **2001**, *357*, 221-228.

9. Pikin, S.A. *Structural Transformations in Liquid Crystals*; Taylor & Francis: New York, NY, USA, 1991.
10. Lavreontovich, O.D.; Pergamenschchik, V.M. Periodic structures in nematic thin-layers. *Pisma V. Zhur. Tekh. Fiz.* **1989**, *15*, 73-78.
11. Lavreontovich, O.D.; Pergamenschchik, V.M. Periodic domain-structures in thin hybrid nematic layers. *Mol. Cryst. Liquid Cryst.* **1990**, *179*, 125-132.
12. Moriya, T. Anisotropic superexchange interaction and weak ferromagnetism. *Phys. Rev.* **1960**, *120*, 91-98.
13. Coffey, D.; Rice, T.M.; Zhang, F.C. Dzyaloshinskii-Moriya interaction in the cuprates. *Phys. Rev. B.* **1991**, *44*, 10112-10116.
14. Bogdanov, A.N.; Rössler, U.K.; Wolf, M.; Müller, K.-H. Magnetic structures and reorientation transitions in noncentrosymmetric uniaxial antiferromagnets. [arXiv:cond-mat/0206291, 2002]
15. Lifschitz, E.M. On the theory of second-order phase transitions. *Zh. Eksp. Teor. Fiz.* **1941**, *11*, 255-269.
16. Sparavigna, A.; Strigazzi, A.; Zvezdin, A.K. Electric-field effects on the spin-density wave in magnetic ferroelectrics. *Phys. Rev. B* **1994**, *50*, 2953-2957.
17. de Sousa, R.; Moore, J.E. Optical coupling to spin waves in the cycloidal multiferroic BiFeO₃. [arXiv:0706.1260v2, 2007]
18. Bobylev, Y.P.; Chigrinov, V.G.; Pikin, S.A. Threshold flexoelectric effect in nematic liquid crystals. *J. Phys.* **1979**, *40*, 331.
19. Meyer, R.B. Piezoelectric effects in liquid crystals. *Phys. Rev. Lett.* **1969**, *22*, 918-921.
20. Maranganti, R.; Sharma, N.D.; Sharma, P. Electromechanical coupling in non piezoelectric materials due to nanoscale nonlocal size effects: Green's function solutions and embedded inclusions. *Phys. Rev. B* **2006**, *74*, 014110:1-014110:14.
21. Lagerwall, S.T. Ferroelectrics: ferroelectric and antiferroelectric. *Liq. Cryst.* **2004**, *301*, 15-45.
22. Clark, N.A.; Lagerwall, S.T. Submicrosecond bistable electro-optic switching in liquid crystals. *Appl. Phys. Lett.* **1980**, *36*, 899-901.
23. Weissflog, W.; Lischka, C.; Diele, S.; Pelzl, G.; Wirth, I.; Grande, S.; Kresse, H.; Schmalfluss, H.; Hartung, H.; Stettler, A. Banana-shaped or rod-like mesogens? Molecular structure, crystal structure and mesophase behaviour of 4,6-dichloro-1,3-phenylene. *Mol. Cryst. Liq. Cryst.* **1999**, *333*, 203-235.
24. Benguigui, L.; Jacobs, A.E. Reentrant smectic-C and smectic-C* phases in liquid crystals under an electric field. *Phys. Rev. E* **1994**, *49*, 4221-4227.
25. Sparavigna, A.; Lavrentovich, O.D.; Strigazzi, A. Periodic stripe domains and hybrid-alignment regime in nematic liquid crystals: Threshold analysis. *Phys. Rev. E* **1994**, *49*, 1344-1352.
26. Barbero, G.; Sparavigna, A.; Strigazzi, A. The structure of the distortion free-energy density in nematics: Second-order elasticity and surface terms. *Nuovo Cim. D* **1990**, *12*, 1259-1272.
27. Frank, F.C. On the theory of liquid crystals. *Discuss. Faraday Soc.* **1958**, *25*, 19-28.
28. Lubensky, T.C. Molecular description of nematic liquid crystals. *Phys. Rev. A* **1970**, *2*, 2497-2514.
29. Nehring, J.; Saupe, A. On the elastic theory of uniaxial liquid crystals. *J. Chem. Phys.* **1971**, *54*, 337-343.

30. Pergamenschik, V.M. Surface-like-elasticity-induced spontaneous twist deformations and long-wavelength stripe domains in a hybrid nematic layer. *Phys. Rev. E* **1993**, *47*, 1881-1892.
31. Lelidis, I.; Barbero, G. Modulated structures in nematic monolayers formed by symmetric molecules. *Phys. Rev. E* **2005**, *71*, 022701:1-022701:4.
32. Helfrich, W. Z. Elastic properties of lipid bilayers: theory and possible experiments. *Z. Naturforschung*, **1973**, *28c*, 693-703.
33. Parthasarathy, R.; Groves, J.T. Curvature and spatial organization in biological membranes. *Soft Matter* **2007**, *3*, 24-33.
34. Barbero, G.; Evangelista, L.R. *An Elementary Course on the Continuum Theory for Nematic Liquid Crystals*; World Scientific: Singapore, 2001.
35. Cheung, D.L.G. *Structures and Properties of Liquid Crystals and Related Molecules from Computer Simulation*; Ph.D Thesis, University of Durham: Durham, UK, 2002.
36. Schmidt, D.; Schadt, M.; Helfrich, W.Z. Liquid-crystalline curvature electricity: The bending mode of MBBA. *Z. Naturforschung*, **1972**, *27a*, 277-280.
37. Barbero, G.; Valabrega, P.T.; Bartolino, R.; Valenti, B. Flexoelectricity in the hybrid aligned nematic cell. *Liq. Cryst.* **1986**, *1*, 483-490.
38. Dozov, I.; Martinot-Lagarde, P.; Durand, G. Flexoelectrically controlled twist of texture in a nematic liquid crystal. *J. Phys. Lett.* **1982**, *43*, L365-L370.
39. Warriar, S.; Madhusudana, N.V. An AC electrooptic technique for measuring the flexoelectric coefficient and anchoring energies of nematics. *J. Phys. II* **1997**, *7*, 1789-1803.
40. Blinov, L.M.; Barnik, M.I.; Ohoka, H.; Ozaki, M.; Yoshino, K. Separate measurements of the flexoelectric and surface polarization in a model nematic liquid crystal p-methoxybenzylidene-p'-butylaniline: Validity of the quadrupolar approach. *Phys. Rev. E* **2001**, *64*, 031707:1-031707:4.
41. Harden, J.; Mbanda, B.; Éber, N.; Fodor-Csorba, K.; Sprunt, S.; Gleeson, J.T.; Jáklí, A. Giant flexoelectricity of bent-core nematic liquid crystals. *Phys. Rev. Lett.* **2006**, *97*, 157802:1-157802:4.
42. Barberi, R.; Barbero, G.; Gabbasova, Z.; Zvezdin, A. Flexoelectricity and alignment phase transitions in nematic liquid crystals. *J. Phys. II* **1993**, *3*, 147-164.
43. Sparavigna, A.; Wolf, R.A. Electron and ion densities in corona plasma. *Czech. J. Phys.* **2006**, *56*, B1062-B1067.
44. Barbero, G.; Strigazzi A. Influence of the surface-like volume elasticity on the critical thickness of a hybrid aligned nematic cell. *J. Phys. Lett.* **1984**, *45*, L857-L862.
45. Palto, S.P.; Mottram, N.J.; Osipov, M.A. Flexoelectric instability and a spontaneous chiral-symmetry breaking in a nematic liquid crystal cell with asymmetric boundary conditions. *Phys. Rev. E* **2007**, *75*, 061707:1-061707:8.
46. Belavin, A.A.; Polyakov, A.M. Metastable states of 2-dimensional isotropic ferromagnets. *JETP Lett.* **1975**, *22*, 245-247.
47. Abdullaev, F.K.; Galimzyanov, R.M.; Kirakosyan, A.S. Local magnon modes and resonances for dynamical skyrmions in Heisenberg two-dimensional ferromagnets. *Phys. Rev. B*, **1999**, *60*, 6552-6557.